J. Fluid Mech. (2010), *vol.* 658, *pp.* 229–246.
doi:10.1017/S0022112010001655

On the role of gravity and shear on inertial particle accelerations in near-wall turbulence

V. LAVEZZO[1], A. SOLDATI[1] S. GERASHCHENKO[2], Z. WARHAFT[2] AND L. R. COLLINS[2]†

[1]Dipartimento di Energetica e Macchine, Università degli Studi di Udine, 33100 Udine, Italy

[2]Sibley School for Mechanical and Aerospace Engineering, Cornell University, Ithaca, NY 14853, USA

(Received 25 September 2009; revised 1 April 2010; accepted 1 April 2010; first published online 15 June 2010)

Recent experiments in a turbulent boundary layer by Gerashchenko *et al.* (*J. Fluid Mech.*, vol. 617, 2008, pp. 255–281) showed that the variance of inertial particle accelerations in the near-wall region increased with increasing particle inertia, contrary to the trend found in homogeneous and isotropic turbulence. This behaviour was attributed to the non-trivial interaction of the inertial particles with both the mean shear and gravity. To investigate this issue, we perform direct numerical simulations of channel flow with suspended inertial particles that are tracked in the Lagrangian frame of reference. Three simulations have been carried out considering (i) fluid particles, (ii) inertial particles with gravity and (iii) inertial particles without gravity. For each set of simulations, three particle response times were examined, corresponding to particle Stokes numbers (in wall units) of 0.9, 1.8 and 11.8. Mean and r.m.s. profiles of particle acceleration computed in the simulation are in qualitative (and in several cases quantitative) agreement with the experimental results, supporting the assumptions made in the simulations. Furthermore, by comparing results from simulations with and without gravity, we are able to isolate and quantify the significant effect of gravitational settling on the phenomenon.

Key words: boundary layers, particle/fluid flows, simulation

1. Introduction

Particle or droplet interactions with turbulence are important in many environmental flows (e.g. cloud formation, atmospheric transport and ocean sediment transport) as well as industrial applications (e.g. combustion devices, aerosol drug delivery and powder manufacturing). Turbulence itself is an inherently complex and highly intermittent phenomenon that exhibits wide temporal and spatial variations in its properties (e.g. Frisch 1995). With respect to particle motions, turbulence is known to enhance the rate of mixing or dispersion of particles (Salazar & Collins 2009), collision/coalescence (Sundaram & Collins 1997) and gravitational settling for particles heavier than the surrounding fluid (Wang & Maxey 1993).

Recent advances in particle tracking capabilities based on optical techniques (Voth *et al.* 2001; Hoyer *et al.* 2005; Ouellette, Xu & Bodenschatz 2006) and acoustic techniques (Mordant *et al.* 2005) have enabled the experimental quantification of individual particle velocity (Mordant *et al.* 2001, 2003; Chevillard *et al.* 2005; Xu

† Email address for correspondence: lc246@cornell.edu

et al. 2006) and acceleration (La Porta *et al.* 2001; Mordant, Crawford & Bodenschatz 2004*a*, *b*; Berg 2006) statistics, including effects due to the finite size of the particles (Qureshi *et al.* 2007; Brown, Warhaft & Voth 2009), particle inertia (Ayyalasomayajula *et al.* 2006; Volk *et al.* 2008*a*, *b*) and polymers dissolved in the fluid (Liberzon *et al.* 2005; Crawford *et al.* 2008; Ouellette, Xu & Bodenschatz 2009). Tracking of multiple particles has yielded measurements of two-particle dispersion (Ott & Mann 2000; Bourgoin *et al.* 2006) and velocity-gradient statistics in the Lagrangian frame (Guala *et al.* 2005, 2007). See Salazar & Collins (2009) and Toschi & Bodenschatz (2009) for recent reviews of multi-particle Lagrangian measurements.

The acceleration of a particle is related to the net force it experiences along its trajectory through Newton's law: $\boldsymbol{a} \equiv \mathrm{d}\boldsymbol{v}/\mathrm{d}t = 1/m \sum_i \boldsymbol{F}_i$, where $\boldsymbol{v}$ is the velocity, $\boldsymbol{a}$ is the acceleration, m is the mass and $\boldsymbol{F}_i$ is the ith force acting on the particle. For a deformable continuum, the acceleration of a fluid point is given by the substantial derivative of the velocity, i.e. $\boldsymbol{a} \equiv \mathrm{D}\boldsymbol{u}/\mathrm{D}t = \partial \boldsymbol{u}/\partial t + \boldsymbol{u}\cdot\boldsymbol{\nabla}\boldsymbol{u}$, where $\boldsymbol{u}$ is the fluid velocity. Furthermore, if the fluid is Newtonian and satisfies the Navier–Stokes equation, the particle acceleration is related to the normal and viscous stresses through $\boldsymbol{a} = -\boldsymbol{\nabla} p/\rho + \nu\nabla^2\boldsymbol{u}$, where p is the pressure, ρ is the fluid density and ν is the kinematic viscosity. Experimental measurements of 'fluid particles' (small nearly neutrally buoyant particles) show remarkably broad tails in the acceleration probability density function (p.d.f.) (Voth *et al.* 2002; Mordant *et al.* 2004*a*). Prediction of these broad tails has been the subject of numerous theoretical studies (Beck 2001*a*, *b*; Reynolds 2003; Reynolds *et al.* 2005). An investigation of acceleration p.d.f. statistics by Biferale & Toschi (2006) revealed a strong correlation between the tails of the distribution and the trapping of fluid particles in vortices. By studying the behaviour of particles in isotropic turbulence using direct numerical simulation (DNS), they demonstrated that the fluid particle acceleration is sensitive to the confinement of particles for relatively long periods of time within the relatively rare small-scale vortex filaments.

For particles that are denser than the surrounding fluid, it becomes necessary to account for the effect of their inertia on the particle trajectory. It is well known that particle behaviour in this regime is characterized by the particle Stokes number, which is the ratio of the particle relaxation time $\tau_p \equiv \beta d^2/18\nu$ to an appropriately chosen fluid time scale, where $\beta \equiv \rho_p/\rho$ is the ratio of the particle density to the fluid density and d is the particle diameter. For homogeneous isotropic turbulence, the fluid time scale chosen is often the Kolmogorov time scale defined as $\tau_\eta \equiv (\nu/\epsilon)^{1/2}$, where ϵ is the turbulent kinetic energy dissipation rate. The resulting Stokes number will be designated as $St_\eta \equiv \tau_p/\tau_\eta$. A particle of infinitesimally small Stokes number will behave like a fluid particle, while the motion of particles with finite Stokes number will systematically deviate from that of a fluid particle with increasing Stokes number.

The acceleration statistics for polydispersed 'inertial particles' have been measured in a wind tunnel (Ayyalasomayajula *et al.* 2006) and with DNS (Bec *et al.* 2006), and they both show that the acceleration variance decreases and the p.d.f. becomes narrower with increasing Stokes number. The explanation appears to be related to two physical effects of the particle inertia, each of which depends upon Stokes number: (i) inertia causes the particles to be centrifuged out of vortices and to collect in high-strain regions of the fluid (Eaton & Fessler 1994), referred to as 'sampling', and (ii) inertial particles have an attenuated response to fluid particle accelerations, referred to as 'filtering'. Bec *et al.* (2006) argued that at smaller Stokes number, the biased sampling resulting from the centrifuge effect dominates, causing the particles to avoid the vortex filaments where the most extreme acceleration events occur (Biferale &

Toschi 2006). As a result, inertial particles experience larger acceleration events at a reduced rate. Ayyalasomayajula, Warhaft & Collins (2008) suggested that it is precisely the coupling between sampling and filtering that has a profound impact on the statistics. By means of Lagrangian tracking of inertial particles in synthetic isotropic turbulence formed by a two-dimensional array of potential-flow vortices, they observed results consistent with the DNS and experiments, namely that with increasing particle inertia the variance of acceleration decreased and the p.d.f. became narrower. They showed that filtering too affected the shape of the p.d.f., as the time scale of the acceleration event is a function of its magnitude, causing a bias in the filtering by inertia that further attenuates the tail.

The centrifuge effect that causes inertial particles to cluster in homogeneous isotropic turbulence is robust, holding under circumstances when the turbulence is subject to a strong mean shear, as confirmed by numerous authors for channel flow (e.g. see Rouson & Eaton 2001). In a channel flow, these structures mainly correspond to streamwise counter-rotating vortices close to the wall, related to the sweeps and ejections that characterize wall-bounded flows (Adrian, Meinhart & Tomkins 2000). Using high-speed Lagrangian particle tracking to investigate the motion of water droplets in a horizontal turbulent boundary layer, Gerashchenko *et al.* (2008) revealed unexpected trends for inertial particle accelerations in the near-wall region; they observed an increase in the acceleration variance with increasing Stokes number, contrary to what was found with inertial particles in isotropic turbulence. They conjectured that this reversal in the trend is the result of the complex interactions of the inertial particles with mean shear and gravity. However, due to the experimental nature of the study, they were not able to separate the contribution of these two forces to verify their hypothesis.

The goal of this study is to apply DNS of a horizontal channel flow with suspended inertial particles that are tracked in a Lagrangian frame of reference to study inertial particle acceleration statistics in the near-wall region of the flow. Parameters have been chosen to match, as closely as possible, the experiments of Gerashchenko *et al.* (2008), enabling a straightforward comparison between the two. Previous numerical studies on particle-laden channel flows have examined the modification of particle velocity statistics due to the presence of coherent structures (Marchioli & Soldati 2002), gravity and shear (Marchioli, Picciotto & Soldati 2007) and preferential concentration (Rouson & Eaton 2001). However, to our knowledge, there has been no attempt to analyse the effects of gravity and shear on particle acceleration statistics. We can isolate the effect of gravity by eliminating this force and by observing how this impacts the acceleration statistics of the particles.

This paper is organized as follows. The details of the numerical simulations, numerical methods and parameter selection are presented in § 2; the results of the comparison between the experiments of Gerashchenko *et al.* (2008) and our DNS are given in § 3; and finally conclusions are presented in § 4.

2. Methodology

2.1. *Governing equations*

We consider an incompressible Newtonian fluid, confined between two horizontal parallel walls, that is undergoing turbulent flow such that the flow is statistically homogeneous in the streamwise (x) and spanwise (y) directions, and inhomogeneous in the wall-normal direction (z). The equations for the fluid are the continuity and

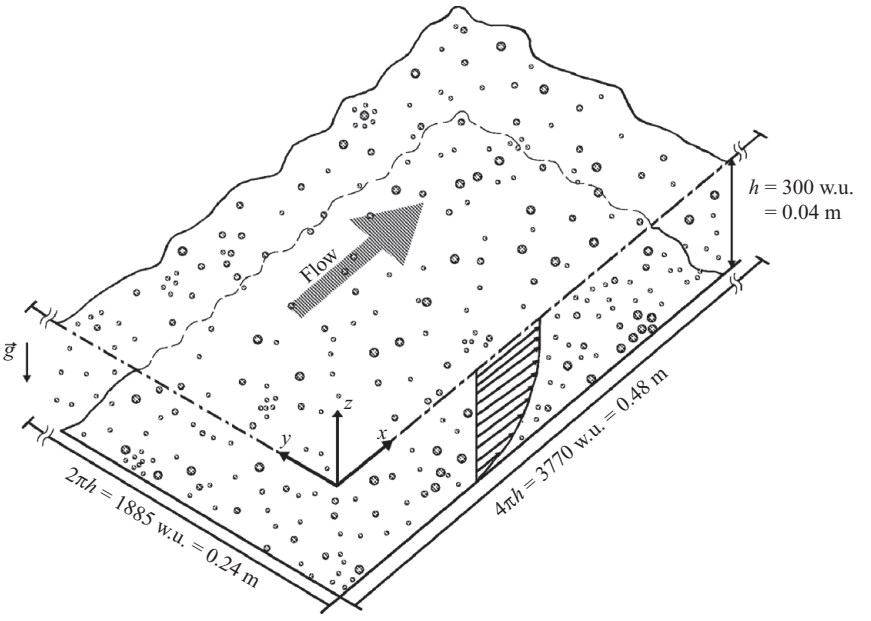

FIGURE 1. Lower half of the domain used in the channel flow DNS. Channel dimensions expressed in wall units (w.u.) are $4\pi h$ in the streamwise (x) direction, $2\pi h$ in the spanwise (y) and $2h$ in the wall-normal (z) direction with $h = 300$. A grid with $256 \times 256 \times 257$ points in the x, y and z directions, respectively, has been used to discretize the domain.

Navier–Stokes equations, respectively, shown below:

$$\nabla \cdot \boldsymbol{u} = 0, \tag{2.1}$$

$$\frac{\partial \boldsymbol{u}}{\partial t} + \boldsymbol{u} \cdot \nabla \boldsymbol{u} = -\frac{\nabla p}{\rho} + \nu \nabla^2 \boldsymbol{u}. \tag{2.2}$$

The domain of the flow, shown schematically in figure 1, is a horizontal channel bounded by two walls of length $4\pi h$ in the x direction, $2\pi h$ in the y direction and separated by a distance $2h$ in the z direction, where $h = 0.04$ m (the maximum achievable height for this combination of parameters, computational resources and grid resolution). The fluid parameters are chosen to match air ($\rho = 1.2\,\mathrm{kg\,m^{-3}}$, $\nu = 1.5 \times 10^{-5}\,\mathrm{m^2\,s^{-1}}$).

Into this fluid, we have uniformly and randomly distributed 320 000 water droplets ($\rho_p = 1000\,\mathrm{kg\,m^{-3}}$), with three different diameters, throughout the domain. The droplets satisfy the following equations of motion (Maxey & Riley 1983):

$$\frac{\mathrm{d}\boldsymbol{x}}{\mathrm{d}t} = \boldsymbol{v}, \tag{2.3}$$

$$\frac{\mathrm{d}\boldsymbol{v}}{\mathrm{d}t} = \frac{\boldsymbol{u} - \boldsymbol{v}}{\tau_p}\left(1 + 0.15 Re_p^{0.687}\right) - \left(1 - \frac{1}{\beta}\right)\boldsymbol{g}, \tag{2.4}$$

where $\boldsymbol{x}$ and $\boldsymbol{v}$ are the particle position and velocity, respectively, $\tau_p = \beta d^2/18\nu$ is the particle response time, $\beta = \rho_p/\rho$ is the particle-to-fluid density ratio, d is the particle diameter, $Re_p = d|\boldsymbol{u} - \boldsymbol{v}|/\nu$ is the local particle Reynolds number and $\boldsymbol{g}$ is the gravitational vector. We assume that the drag force and gravity are the dominant forces, and neglect the other terms in the Maxey & Riley relationship under the assumptions that the particles are small (i.e. $d/\eta < 1$, where η is the Kolmogorov

length scale) and have a large density ratio (i.e. $\beta = 833 \gg 1$) (Elghobashi & Truesdell 1992). We include the local-Reynolds-number correction of Schiller & Neumann (1933) to account for finite-Reynolds-number effects on the drag coefficient, even though the local Reynolds numbers are generally small ($Re_p < 1$ for all the Stokes number cases we simulate).

For the case of a fluid particle (zero inertia), the particle velocity is replaced by the fluid velocity at the point, yielding the kinematic relationship

$$\frac{\mathrm{d}\boldsymbol{x}}{\mathrm{d}t} = \boldsymbol{u}. \tag{2.5}$$

2.2. *Numerical method*

The Navier–Stokes equations are solved on a Cartesian grid with $256 \times 256 \times 257$ grid points in the x, y and z directions, respectively. The code is based on a pseudospectral algorithm that decomposes the velocity into Fourier modes in the x and y directions and Chebyshev polynomials in the inhomogeneous z direction. Periodic boundary conditions are imposed in the streamwise (x) and spanwise (y) directions and no-slip boundary conditions are enforced at the upper and lower walls. Details of the numerical method can be found in earlier publications (Soldati & Banerjee 1998; Picciotto, Marchioli & Soldati 2005). Simulations with $\Delta t = 10^{-4}$ were performed for long times until a stationary turbulence state was achieved.

Particles are initially placed at random locations throughout the domain and are assigned the fluid velocity corresponding to their position. They are advanced in a Lagrangian frame of reference based on (2.3) and (2.4). As the particle loadings are very low, the effect of turbulence modulation by the particles (Elghobashi & Truesdell 1993; Sundaram & Collins 1999) and particle–particle collisions (Sundaram & Collins 1997) have been neglected. A fourth-order Runge–Kutta scheme is used to integrate the governing equations in time and sixth-order Lagrangian polynomials are employed to interpolate the fluid velocity to the particle positions. Periodic boundary conditions are imposed on the particle trajectories in the streamwise and spanwise directions. At the channel walls, the particles are assumed to undergo elastic collisions that conserve the incident particle momentum and energy.

2.3. *Parameters*

The parameters in the DNS have been chosen to optimize the comparison with the experiment of Gerashchenko *et al.* (2008). Although the units in a DNS are arbitrary, the numerical values have been chosen to match those of the experiment at the lower Reynolds number in MKS units (see table 1). As we are especially concerned with the particle behaviour in the near-wall region, we decided to closely match the friction velocity. This way, the flow in the near-wall region should closely correspond to the experiment. Far from the wall, the flows in the simulations and experiments deviate; the experimental flow is a zero-pressure-gradient boundary layer with an outer flow that contains high levels of free-stream turbulence, whereas the DNS is that of a classical channel flow. While there is some correspondence between the two, in that there is turbulence in the outer flow that is not found with a classical boundary layer, the two streams approach different outer flow turbulence conditions. Therefore, it was not possible to simultaneously match the wall friction velocity and the free-stream turbulence, and so the latter was not matched in the DNS. This discrepancy is evident in the shear Reynolds number. In the DNS, the shear Reynolds number is given by $Re_\tau = u_\tau h/\nu = 300$, whereas in the boundary-layer experiment $Re_\tau \equiv u_\tau \delta/\nu = 470$ and 833 for the low- and high-Reynolds-number cases, respectively. Note that we

Name	u_τ (m s^{-1})	Height (m)	Re_τ	g^+	d (μm)	St
DNS						
Low	0.112	$h=0.04$	300	0.111	18.4	0.87
Medium	0.112	$h=0.04$	300	0.111	26.1	1.76
High	0.112	$h=0.04$	300	0.111	67.6	11.8
Gerashchenko *et al.* (2008)						
Low	0.117	$\delta=0.06$	470	0.091	16	0.72
Medium	0.124	$\delta=0.1$	833	0.077	16	0.81
High	0.124	$\delta=0.1$	833	0.077	41	5.3

TABLE 1. Fluid and particle parameters from the simulations and the experiments of Gerashchenko *et al.* (2008) as indicated. The fluid (air) density and viscosity were taken to be 1.2 kg m^{-3} and 1.5×10^{-5} m^2 s^{-1}, respectively. Gravity was set to 9.81 m s^{-1} and the density of water was 1000 kg m^{-3}, corresponding to a particle-to-fluid density ratio $\beta=833$.

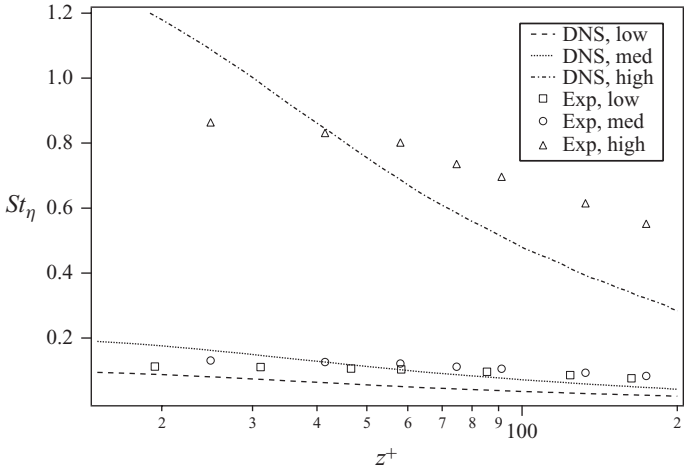

FIGURE 2. Variation of St_η over the experimental boundary layer (points) and DNS (lines). $z^+\equiv zu_\tau/\nu$ is the dimensionless distance from the wall, where $u_\tau=\sqrt{\tau_w/\rho}$ and τ_w is the average shear stress at the wall.

are using the standard definition for the friction velocity in wall-bounded flows, $u_\tau\equiv\sqrt{\tau_w/\rho}$, where τ_w is the average shear stress at the wall. It has been found over the range of Reynolds numbers studied that the Reynolds number has little effect on the particles in the near-wall region (Marchioli *et al.* 2007) and hence we are not concerned with this discrepancy. The gravitational vector is important for the settling particles. Its value was set to 9.81 m s^{-2}, corresponding to a dimensionless gravitational acceleration $g^+\equiv g\nu/u_\tau^3$ of 0.111 in the DNS and 0.091 and 0.077 at the two experimental conditions, respectively.

As discussed previously, the Stokes number is a key parameter for describing the particle inertia and hence this parameter must be chosen carefully in the DNS. We define the Stokes number in wall units as $St\equiv\tau_p u_\tau^2/\nu$. The values for the experiment and DNS are given in table 1. Because the outer flow conditions for the boundary layer and DNS were not the same, it was not possible to precisely match the Stokes numbers in the two flows (see figure 2). Moreover, the droplets in the experiment were polydisperse in size, whereas the droplets in the DNS were monodisperse. We decided

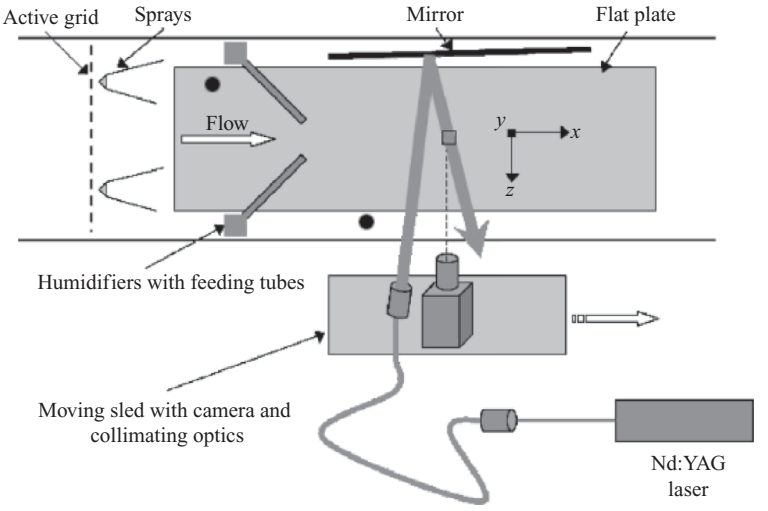

FIGURE 3. Experimental set-up of Gerashchenko *et al.* (2008) (top view). The two separate methods of introducing the droplets are shown together. When the sprays are operating, the humidifiers and feeding tubes are removed from the tunnel. The y coordinate is measured vertically from the plate.

that the optimal approach would be to set τ_p in the DNS so as to achieve as good an overlap in St_η as possible, with an emphasis on the inner boundary layer over the outer boundary layer since the comparisons are focused predominantly on the inner layer. We reiterate that conditions in the experiment were achieved by varying both the flow conditions (Re_τ) and the droplet size, whereas in the DNS the flow was fixed and only the droplet size (Stokes number) was varied. Hereafter we shall refer to the three cases as the high-, medium- and low-Stokes-number cases. Figure 2 shows a comparison of the variation in the local St_η across the two flows, demonstrating the qualitative correspondence we achieve with the three experimental conditions.

2.4. *Experimental set-up*

To provide a self-contained discussion of the comparisons, we include a brief summary of the experimental technique. Figure 3 shows a sketch of the experimental set-up. The facility consists of an open-loop wind tunnel with dimensions $1 \times 0.9 \times 20$ m^3 outfitted with either a passive grid or an active grid capable of generating intense turbulence (Mydlarski & Warhaft 1996). The boundary layer is formed on a flat glass plate placed 40 cm above the tunnel floor (grey rectangle in the centre of the figure). Sprays or humidifiers were placed 3.6 and 2 m upstream from the observation region respectively to generate the droplets at a mass loading of 10^{-4} kg water per kg air. A high-speed camera attached to a precision, linearly translating, pneumatically driven sled (Gylfason 2006) was employed to accurately track the droplets in the boundary layer for a total distance of approximately 50 cm. Particle accelerations were computed by convolving the particle position measurements with a kernel that filters and twice differentiates (in time) the data. These data are then binned according to their distance above the plate for later processing. Additionally, supplementary measurements of two components of the velocity in the boundary layer were made using laser Doppler velocimetry (LDV) and hot wire anemometry (HWA). To study the effects of inertia as well as turbulence on particle behaviour, two experiments were considered: one

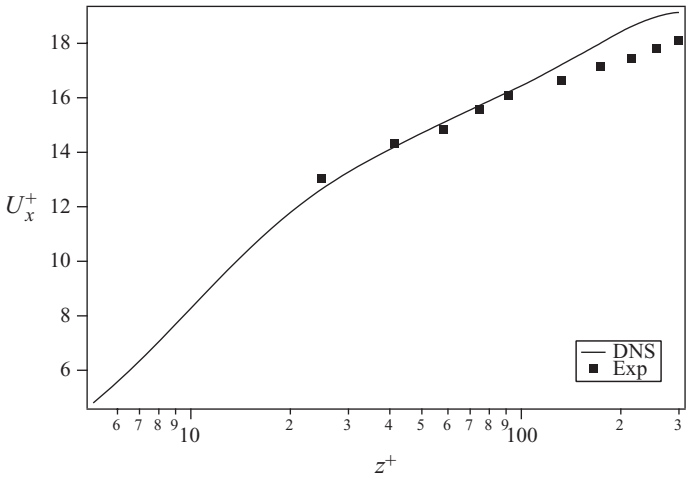

FIGURE 4. Mean streamwise fluid velocity profile in standard wall units (non-dimensionalized by the friction velocity). The line is from the DNS at $Re_\tau = 300$ and the ■ symbols are the experimental data at $Re_\tau = 470$. Note that the velocity profiles were only measured down to $z^+ \sim 25$ using hot wires. Particle accelerations (discussed below) measured using a particle tracking technique reached closer to the wall.

Reynolds number with two droplet Stokes numbers and one Stokes number at two different Reynolds numbers. Further details of the methodology and the measuring techniques can be found in Gerashchenko *et al.* (2008).

3. Results and discussion

The objectives of this section are: (i) to compare inertial particle acceleration statistics from the simulations with the experiments and (ii) to investigate the role of gravitational settling on inertial particle acceleration statistics. Before discussing results for the particle accelerations, we compare the simulation and experimental mean fluid velocity. Figure 4 shows a comparison of the mean streamwise velocity as a function of the distance from the wall in wall units and using the standard 'law-of-the-wall' coordinates. Throughout this section, lines refer to the simulation results and symbols correspond to experimental measurements. There is good agreement between the DNS and experiments for $z^+ \lesssim 100$. Substantial deviations occur at larger separations most likely due to differences in the flow specifications (channel flow versus a boundary layer with free-stream turbulence). This suggests that meaningful comparisons will be limited to this near-wall region of the flow.

Once the DNS had reached a stationary state, the particles were released into the fluid at evenly distributed locations. We refer to this time as $t^+ = 0$ or the initial condition for the particles, where $t^+ \equiv u_\tau^2 t/\nu$ is time in wall units. Particles will settle towards the lower wall under the influence of gravity. Because the flow is homogeneous in the streamwise direction, this settling continues indefinitely until eventually all of the particles deposit onto the wall forming a stagnant layer. As this is physically inconsistent with the experiment, which was inhomogeneous, but stationary, there is a window of time in the simulations over which meaningful comparisons may be made. By examining the particle statistics as a function of time, we discovered empirically that the time window for meaningful comparisons is $35 \leqslant t^+ \leqslant 600$. After this period,

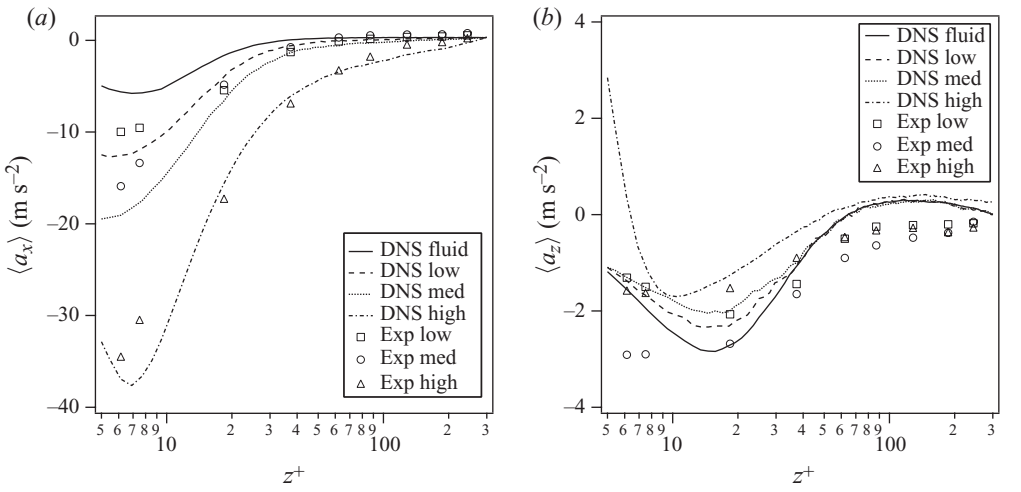

FIGURE 5. Mean particle acceleration in the (*a*) streamwise and (*b*) wall-normal directions as a function of z^+. Lines and symbols represent the simulation and experiments at low, medium and high Stokes numbers, as indicated (see table 1 for details).

the statistics for the highest Stokes number particles become noticeably affected by the particles that have collected on the lower wall.

3.1. *Comparison with experiment*

Figure 5 shows a comparison of the mean streamwise and spanwise accelerations as a function of the wall-normal distance. Overall there is qualitative agreement between the experiments and the simulations at the three values of the particle Stokes number (low, medium and high), and for the case of the streamwise acceleration (figure 5*a*) there is even good quantitative agreement. For the streamwise component of acceleration, there are some deviations observed for $z^+ < 10$; however, this may be the result of difficulties in making the measurements this close to the wall or due to differences in the wall boundary conditions for the particles (the DNS assumed the particles colliding with the wall rebound elastically, whereas droplets in the experiment that impact the wall perhaps coat the surface and do not rebound). Also, the droplets in the experiments have a relatively broad size distribution (see figure 8 in Gerashchenko *et al.* 2008), whereas the particles in the DNS were uniform in size. Results for the wall-normal component shown in figure 5(*b*) agree qualitatively with the experiment, but not quantitatively. The DNS at the lower two values of Stokes number capture the correct shape of the curve, but the highest Stokes number shows a change in sign not found in the experiment. It is very likely that this is due to the effect of the rebounding particles.

Figure 6 shows the r.m.s. of the acceleration fluctuations as a function of the distance from the wall. Once again, the DNS captures most of the qualitative trends with particle Stokes number correctly and is in reasonably good agreement with the experiments, particularly for the streamwise component in the near-wall region. For $z^+ > 100$, the DNS systematically under-predicts the experimental measurements of the streamwise component, but this is most likely due to the difference in the outer flow condition, as already noted. The DNS shows that the streamwise acceleration variance increases with increasing Stokes number for $z^+ \lesssim 25$, as described by Gerashchenko *et al.* (2008). This result confirms the qualitative difference between the wall shear flow

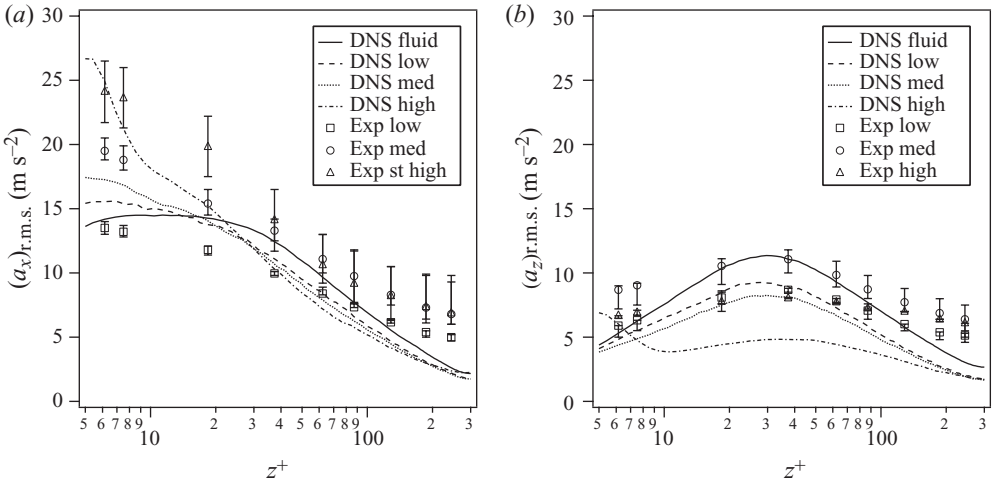

FIGURE 6. Root-mean-square of particle acceleration fluctuations in the (*a*) streamwise and (*b*) wall-normal directions as a function of z^+. Lines represent the DNS results and the symbols are from the experiments at low, medium and high Stokes numbers, as indicated.

and isotropic turbulence, where the opposite trend was observed (Ayyalasomayajula *et al.* 2006; Bec *et al.* 2006). We also observe a reversal in the trend with Stokes number for $z^+ \gtrsim 25$ wall units in the channel flow DNS, most likely due to the diminished effect of the wall and the approach to isotropic turbulence near the centreline. This result is in good agreement with the observations of Choi, Yeo & Lee (2004) on the effects of flow inhomogeneity and anisotropy on particle acceleration in wall-bounded turbulence. This reversal in the trend is not as obvious in the experiment. However, it is important to recall that the lowest Stokes number case in the boundary-layer experiment corresponds to a lower Reynolds number, which is most likely the cause for the suppression of the streamwise acceleration r.m.s. for this case across the entire boundary layer. The medium- and high-Stokes-number cases, which correspond to the same Reynolds number, do show a slight reversal for $z^+ \gtrsim 25$, although the trend is difficult to discern in the light of the size of the error bars (see figure 14 and related text in Gerashchenko *et al.* (2008) for a further discussion of this point). The results for the wall-normal direction shown in figure 6(*b*), much like the results for the mean acceleration in this direction, are only in qualitative agreement, with the greatest disparity shown for the highest Stokes number. Once again we suspect that this could be the influence of the boundary condition for the particles at the wall.

To examine higher order statistics of the acceleration fluctuations, we look at the p.d.f. of particle accelerations in the streamwise and wall-normal directions, in standard coordinates (i.e. acceleration normalized by its r.m.s. value). Figure 7 shows the p.d.f. at four locations: $z^+ = 7.5$, 18, 37 and 244. Note that for visual clarity the p.d.f. at each successive distance is offset vertically by 2 on the logarithmic axis. At all three Stokes numbers, the agreement in the near-wall region is excellent. In particular, the DNS is capturing the shape well. For the low-Stokes-number case, there is a significant discrepancy in the p.d.f.s for $z^+ = 244$. As noted earlier, the flows at that large distance are not matched, and apparently the particle with the smallest Stokes number is the most sensitive to the underlying flow. It is interesting to observe that as the Stokes number increases the p.d.f. tails in this normalized plot become narrower as a consequence of the selective sampling by the particles of the underlying

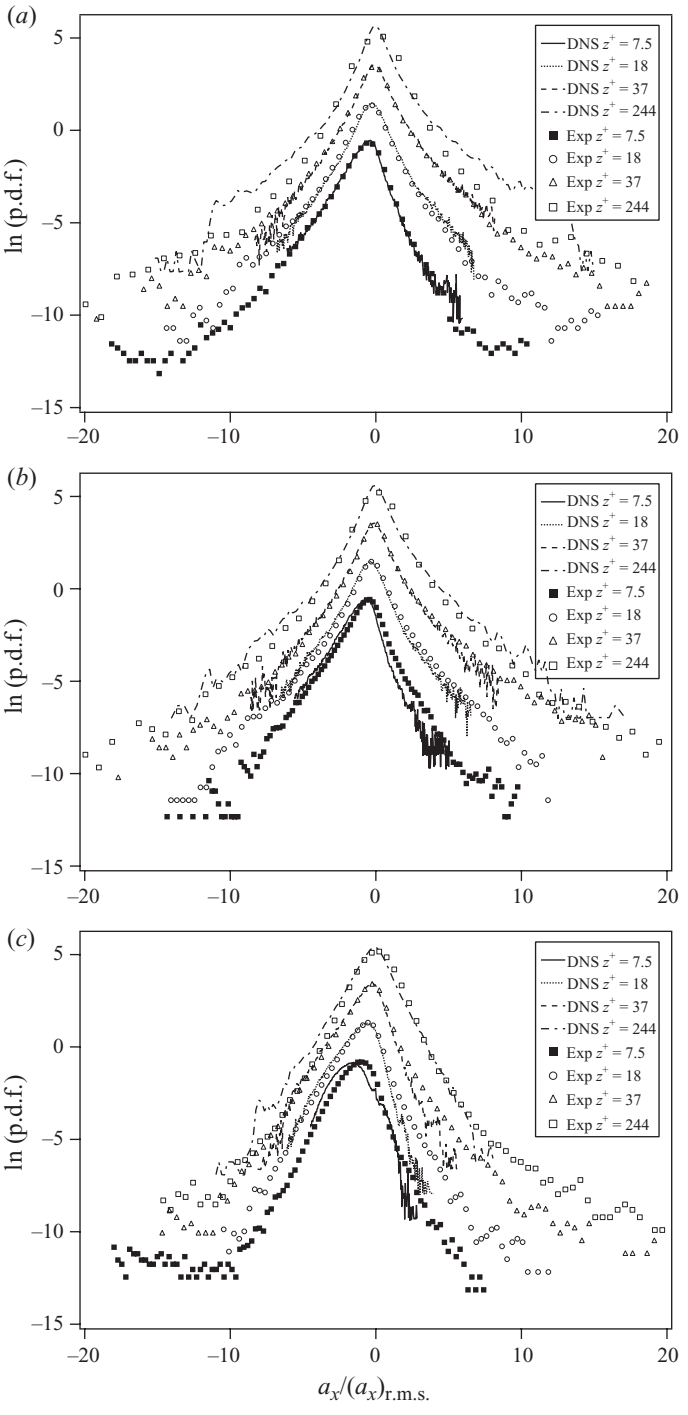

FIGURE 7. Probability density functions of particle accelerations in the streamwise direction at channel heights: $z^+ = 7.5$, 18, 37 and 244 for (*a*) low, (*b*) medium and (*c*) high Stokes numbers. Note that for visual clarity the p.d.f. at each successive distance is offset vertically by 2 on the logarithmic axis. Lines represent the DNS values and the symbols are the experimental data, as indicated.

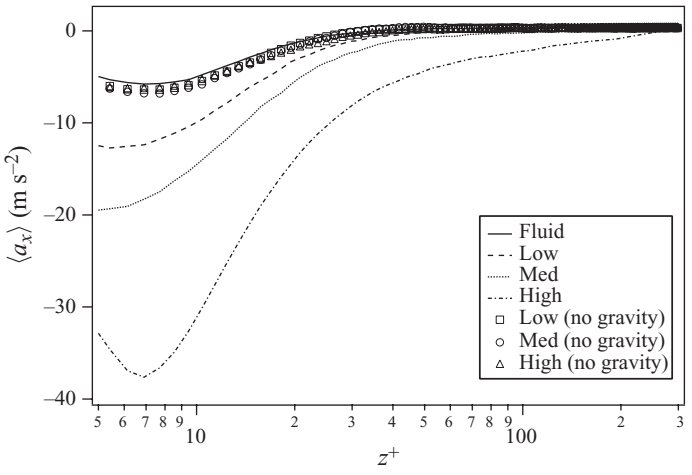

FIGURE 8. Mean particle acceleration in the streamwise direction at the three Stokes numbers, as indicated. Simulations results with gravity (lines) and without gravity (symbols).

fluid velocity field, as described in previous works (e.g. Bec *et al.* 2006; Chen, Gogo & Vassilicos 2006; Ayyalasomayajula *et al.* 2008).

In figure 7, the three Stokes number particles exhibit a common pattern, namely with decreasing distance from the wall, the tails of the p.d.f. become increasing skewed, and the peak is shifted to smaller (more negative) values, consistent with the mean profiles shown earlier. This trend was pointed out by Gerashchenko *et al.* (2008), who related the behaviour to the coupling of the particle motion to the mean shear and gravity. This conjecture will be considered in greater detail in the next section.

3.2. *Effect of gravity*

To isolate the effect of gravity, we re-ran the simulations shown in the previous section without gravity, i.e. with only the Stokes drag force in (2.4) acting on the particles. Overall we observe that the removal of gravity has a profound effect on the particle acceleration statistics. For example, in figure 8 we show the mean acceleration in the streamwise direction and observe that the cases without gravity (symbols) are substantially reduced in magnitude (by more than a factor of 5 for the highest Stokes number case) relative to the runs with gravity (lines); furthermore, the cases without gravity appear to collapse onto the fluid acceleration curve. Apparently it is the coupling with gravitational settling that leads to the large mean decelerations of the droplets near the wall.

To further analyse this behaviour, it is first useful to consider the shape of the mean fluid acceleration in the longitudinal direction. From the Reynolds-averaged Navier–Stokes equations for a steady fully developed flow, we can derive the following relationship:

$$\langle a_x \rangle = \frac{\mathrm{d}\langle u'w' \rangle}{\mathrm{d}z}, \tag{3.1}$$

where $\langle u'w' \rangle$ is the Reynolds stress term acting in the wall-normal direction. Figure 9(*a*) shows a plot of the two sides of (3.1), confirming the relationship. In the light of the good agreement between the mean acceleration for the inertial particles and fluid particles, we conjecture that a similar relationship holds for the

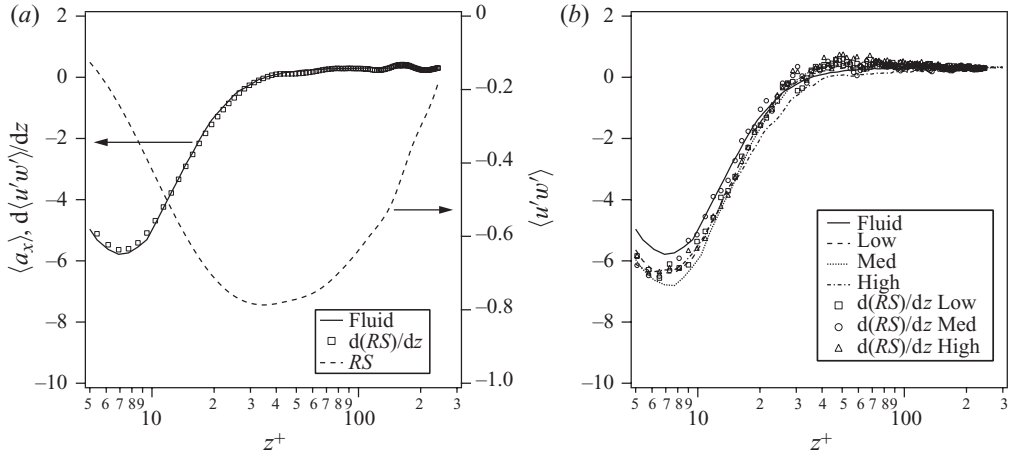

FIGURE 9. Comparison of the mean longitudinal acceleration $\langle a_x \rangle$ (lines) as a function of the distance from the wall with the derivative of the wall-normal component of the Reynolds stress $\mathrm{d}\langle u'w' \rangle/\mathrm{d}z$ (symbols) per (3.1) and (3.2) for (*a*) fluid particle and (*b*) inertial particles at the low, medium and high Stokes numbers, as indicated. Dashed line in (*a*) is the Reynolds stress (*RS*) and uses the axis on the right side of the graph.

inertial particles, i.e.

$$\langle a_{xp} \rangle = \frac{\mathrm{d}\langle u'_p w'_p \rangle}{\mathrm{d}z}, \tag{3.2}$$

where $\langle u'_p w'_p \rangle$ is the particle stress in the wall-normal direction. The equivalent comparison for the inertial particles is shown in figure 9(*b*) and the agreement is nearly as good for all three Stokes numbers. Over the range of Stokes numbers considered, the average acceleration and Reynolds stress of the inertial particles is nearly identical to those of the fluid particle, suggesting that an equilibrium between the mean particle and fluid velocity fields has been established. This has been confirmed in simulations at even higher values of the Stokes number (not shown), so long as particles impacting the walls are removed from the statistical average.

While in the absence of gravity inertia has no effect on the mean particle acceleration, it does influence the acceleration variance. This can be seen in figure 10, which shows the r.m.s. of the longitudinal acceleration as a function of the distance from the wall. Elimination of gravity strongly attenuates the bump in the acceleration r.m.s. near the wall that was seen to increase with increasing Stokes number over the range considered. Moreover, we see a systematic decrease in the maximum acceleration r.m.s. with increasing Stokes number, in contrast to what was found in the simulations with gravity. The qualitative trend without gravity is therefore consistent with what was found for isotropic turbulence, with likely the same explanation (Ayyalasomayajula *et al.* 2006; Bec *et al.* 2006). Thus, the reversal in the trend with Stokes number discussed in § 3.1 is related to the coupling of gravitational settling with the mean shear.

Given the changes in the r.m.s. of the longitudinal acceleration, it would be expected that gravity too would influence the p.d.f. of acceleration. In figure 11, we compare the p.d.f. of inertial particle acceleration with gravity (lines) to the same without gravity (symbols). For visual clarity, we have shifted the p.d.f.s similarly to those in figure 7. The p.d.f.s without gravity are more symmetric than the ones with gravity, suggesting

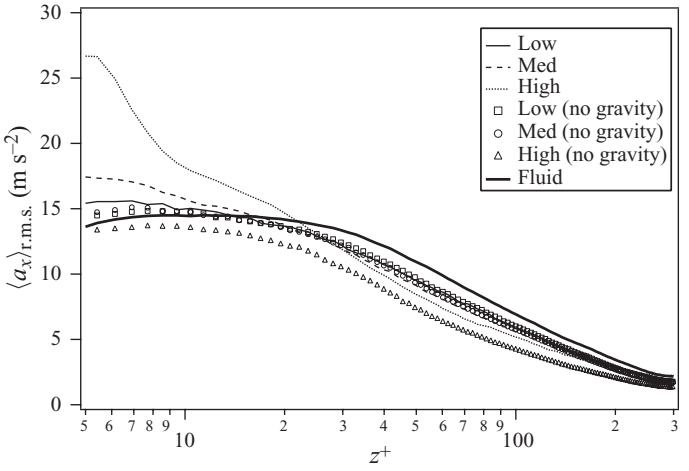

FIGURE 10. Effect of gravity on the r.m.s. of particle acceleration fluctuations in the streamwise direction from the DNS. Simulation results with gravity (lines) and without gravity (symbols) are shown for the three Stokes numbers, as indicated.

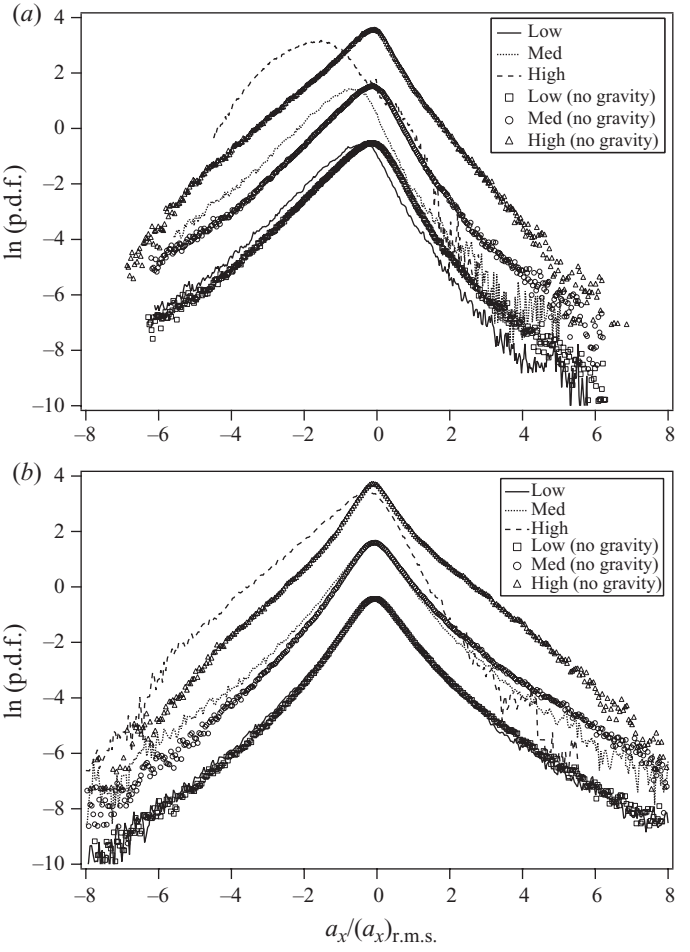

FIGURE 11. Probability density functions of the streamwise component of particle acceleration for the three values of the Stokes numbers with gravity (lines) and without gravity (symbols) at (*a*) $z^+ = 7.5$ and (*b*) $z^+ = 37$. The curves corresponding to the medium and high Stokes numbers are, respectively, shifted upwards by 2 and 4 units for visual clarity.

that gravitational settling contributes significantly to the negative skewness. The effect is most noticeable for the highest Stokes number case, where near the wall gravity is completely reshaping the p.d.f. The effect of gravity on the lower Stokes number particles is more pronounced nearer to the wall ($z^+ = 7.5$). We see a shifting of the curve towards more negative values of acceleration in all three cases. Farther away ($z^+ = 37$), the lowest Stokes number case shows little effect of gravitational settling, while the highest Stokes number case still shows a profound effect.

4. Conclusions

We have used DNS of a turbulent channel flow with Lagrangian particle tracking to study the influence of inertia and gravitational settling on particle acceleration statistics in the near-wall region. The study is motivated by the experimental observations of Gerashchenko *et al.* (2008), who showed a reversal in the trend of particle accelerations with Stokes number compared with isotropic turbulence. Thus, they found that the r.m.s. values increased with increasing Stokes number, in contrast to the decreasing trend found for isotropic turbulence. The parameters in the DNS were chosen to match, as far as possible, those of the experiment of Gerashchenko *et al.* (2008) in the near-wall region. Due to unavoidable differences in the flow specification, it was not possible to precisely match the flow conditions, although this did not significantly impact the near-wall results.

We find that the DNS is able to obtain results in qualitative agreement with the experiments for $z^+ \lesssim 100$. In particular, the DNS is able to replicate the reversal in the trend with particle Stokes number for the variance of the longitudinal and wall-normal acceleration statistics. Furthermore, the DNS is able to obtain p.d.f.s in reasonably good agreement with the experiments over the same range of distances from the wall. While the r.m.s. of the longitudinal acceleration fluctuations increases with increasing particle Stokes number, the p.d.f. of the normalized acceleration decreases, indicating a diminution of strong events by inertia. The DNS also captures the negative skewness of the longitudinal acceleration p.d.f. as a function of the wall-normal distance. This is a stringent test of the main assumption made in the DNS, which is that the near-wall turbulence in the channel flow is similar to the near-wall turbulence in the boundary layer with suitably chosen parameters. For $z^+ > 100$ there are systematic deviations between the DNS and measurements that can be attributed to the differences in the flow at these separations.

One advantage of the DNS is that it is possible to turn off gravitational settling to determine its impact on the particle acceleration statistics. This yielded several interesting findings for the longitudinal acceleration. First, in the absence of gravity, we find that the mean streamwise acceleration of the inertial particles near the wall decreases significantly in magnitude relative to the case with gravity. Furthermore, the profiles for all three Stokes numbers appear to approach that of the fluid particle acceleration. The bump in the curves near the wall observed with gravity disappeared completely. For a fluid particle, we can relate the mean streamwise acceleration to the derivative of the Reynolds stress component acting in the wall-normal direction, and we showed that the same relationship holds for the inertial particles, at least over the range of Reynolds numbers considered in this study. We find the near collapse of the three mean streamwise acceleration curves onto the fluid particle curve puzzling and feel this requires further investigation. Second, the acceleration variance was found to depend on Stokes number in a manner similar to what has been found for particles in isotropic turbulence. The reversal in the trend with Stokes number found

for the acceleration r.m.s. in the streamwise direction by Gerashchenko *et al.* (2008) disappeared. Apparently the increasing acceleration r.m.s. found near the wall with increasing Stokes number in the case of settling particles is due to the coupling of gravity with the mean shear, that is, particles settle towards the wall and experience a stronger deceleration due to the mean shear. Third, the negative skewness in the p.d.f.s of inertial particle accelerations with gravity was found to be greatly diminished when gravity was removed. The effect of gravity on the p.d.f. is most profound for the highest Stokes number case considered ($St = 10.76$). Gravitational settling clearly adds to the phenomenon known as 'crossing trajectories' and this profoundly influences the acceleration statistics of inertial particles in a horizontal boundary layer. Future models of inertial particles must take these effects into account.

V.L. would like to acknowledge Dr C. Marchioli for the helpful technical discussions in the early stages of the study. This work was supported by the National Science Foundation through grant CBET-0756510, by the NASA Microgravity Fluid Physics program grant NNCO5GA45G and by Regione Friuli Venezia Giulia through the grant entitled 'Reducing particulate emissions in the wood industry'. The authors would also like to acknowledge CINECA for the computational resources that were used in this study.

REFERENCES

Adrian, R. J., Meinhart, C. D. & Tomkins, C. D. 2000 Vortex organization in the outer region of the turbulent boundary layer. *J. Fluid Mech.* **422**, 1–54.

Ayyalasomayajula, S., Gylfason, A., Collins, L. R., Bodenschatz, E. & Warhaft, Z. 2006 Lagrangian measurements of inertial particle accelerations in grid generated wind tunnel turbulence. *Phys. Rev. Lett.* **97**, 144507.

Ayyalasomayajula, S., Warhaft, Z. & Collins, L. R. 2008 Modeling inertial particle acceleration statistics in isotropic turbulence. *Phys. Fluids* **20**, 094104.

Bec, J., Biferale, L., Boffetta, G., Celani, A., Cencini, M., Lanotte, A. S., Musacchio, S. & Toschi, F. 2006 Acceleration statistics of heavy particles in turbulence. *J. Fluid Mech.* **550**, 349–358.

Beck, C. 2001*a* Dynamical foundations of nonextensive statistical mechanics. *Phys. Rev. Lett.* **87**, 180601.

Beck, C. 2001*b* On the small-scale statistics of Lagrangian turbulence. *Phys. Lett.* A **27**, 240.

Berg, J. 2006 Lagrangian one-particle velocity statistics in a turbulent flow. *J. Fluid Mech.* **630**, 179–189.

Biferale, L. & Toschi, F. 2006 Joint statistics of acceleration and vorticity in fully developed turbulence. *J. Turbul.* **6** (40), 1–8.

Bourgoin, M., Ouelette, N. T., Xu, H., Berg, J. & Bodenschatz, E. 2006 The role of pair dispersion in turbulent flow. *Science* **311**, 835–838.

Brown, R. D., Warhaft, Z. & Voth, G. A. 2009 Measurement of accelerations of large neutrally-buoyant particles in intense turbulence. *Phys. Rev. Lett.* **103**, 194501.

Chen, L., Gogo, S. & Vassilicos, J. C. 2006 Turbulent clustering of stagnation points and inertial particles. *J. Fluid Mech.* **553**, 143–155.

Chevillard, L., Roux, S. G., Leveque, E., Mordant, N., Pinton, J.-F. & Arneodo, A. 2005 Intermittency of velocity time increments in turbulence. *Phys. Rev. Lett.* **95**, 064501.

Choi, J., Yeo, K. & Lee, C. 2004 Lagrangian statistics in turbulent channel flow. *Phys. Fluids* **16**, 779–793.

Crawford, A. M., Mordant, N., Xu, H. & Bodenschatz, E. 2008 Fluid acceleration in the bulk of turbulent dilute polymer solutions. *New J. Phys.* **10**, 123015.

Eaton, J. K. & Fessler, J. R. 1994 Preferential concentration of particles by turbulence. *Intl J. Multiphase Flow* **20**, 169–209.

Elghobashi, S. E. & Truesdell, G. C. 1992 Direct simulation of a particle dispersion in a decaying isotropic turbulence. *J. Fluid Mech.* **242**, 655.

Elghobashi, S. E. & Truesdell, G. C. 1993 On the two-way interaction between homogeneous turbulence and dispersed particles. Part I. Turbulence modification. *Phys. Fluids* A **5**, 1790–1801.

Frisch, U. 1995 *Turbulence: The Legacy of A. N. Kolmogorov*. Cambridge University Press.

Gerashchenko, S., Sharp, N. S., Neuscamman, S. & Warhaft, Z. 2008 Lagrangian measurements of inertial particle accelerations in a turbulent boundary layer. *J. Fluid Mech.* **617**, 255–281.

Guala, M., Liberzon, A., Tsinober, A. & Kinzelbach, W. 2007 An experimental investigation on Lagrangian correlations of small-scale turbulence at low Reynolds number. *J. Fluid Mech.* **574**, 405–427.

Guala, M., Lüthi, B., Liberzon, A., Tsinober, A. & Kinzelbach, W. 2005 On the evolution of material lines and vorticity in homogeneous turbulence. *J. Fluid Mech.* **533**, 339–359.

Gylfason, A. 2006 Particles, passive scalars, and the small-scale structure of turbulence. PhD thesis, Sibley School of Mechanical & Aerospace Engineering, Cornell University, Ithaca, NY.

Hoyer, K., Holzner, M., Lüthi, B., Guala, M., Liberzon, A. & Kinzelbach, W. 2005 3D scanning particle velocimentry. *Exp. Fluids* **39**, 923–934.

La Porta, A., Voth, G. A., Crawford, A. M., Alexander, J. & Bodenschatz, E. 2001 Fluid particle accelerations in fully developed turbulence. *Nature* **409**, 1017–1019.

Liberzon, A., Guala, M., L uthi, B., Kinzelbach, W. & Tsinober, A. 2005 Turbulence in dilute polymer solutions. *Phys. Fluids* **17**, 031707.

Marchioli, C., Picciotto, M. & Soldati, A. 2007 Influence of gravity and lift on particle velocity statistics and transfer rates in turbulent vertical channel flow. *Intl J. Multiphase Flow* **33**, 227–251.

Marchioli, C. & Soldati, A. 2002 Mechanisms for particle transfer and segregation in a turbulent boundary layer. *J. Fluid Mech.* **468**, 283–315.

Maxey, M. R. & Riley, J. J. 1983 Equation of motion for a small rigid sphere in a nonuniform flow. *Phys. Fluids* **26**, 883–889.

Mordant, N., Crawford, A. M. & Bodenschatz, E. 2004*a* Experimental Lagrangian acceleration probability density function measurement. *Physica* D **193**, 245–251.

Mordant, N., Crawford, A. M. & Bodenschatz, E. 2004*b* Three-dimensional structure of the Lagrangian acceleration in turbulent flows. *Phys. Rev. Lett.* **93**, 214501.

Mordant, N., Delour, J., Leveque, E., Michel, O., Arneodo, A. & Pinton, J.-F. 2003 Lagrangian velocity fluctuations in fully developed turbulence: scaling, intermittency, and dynamics. *J. Stat. Phys.* **113**, 701–717.

Mordant, N., Metz, P., Michel, O. & Pinton, J.-F. 2001 Measurement of Lagrangian velocity in fully developed turbulence. *Phys. Rev. Lett.* **87**, 214501.

Mordant, N., Metz, P., Pinton, J.-F. & Michel, O. 2005 Acoustical technique for Lagrangian velocity measurement. *Rev. Sci. Instrum.* **76**, 025105.

Mydlarski, L. & Warhaft, Z. 1996 On the onset of high-Reynolds-number grid-generated wind tunnel turbulence. *J. Fluid Mech.* **320**, 331–368.

Ott, S. & Mann, J. 2000 An experimental investigation of the relative diffusion of particle pairs in three-dimensional turbulent flow. *J. Fluid Mech.* **422**, 207–223.

Ouellette, N. T., Xu, H. & Bodenschatz, E. 2006 A quantitative study of three-dimensional particle tracking algorithms. *Exp. Fluids* **40**, 301–313.

Ouellette, N. T., Xu, H. & Bodenschatz, E. 2009 Bulk turbulence in dilute polymer solutions. *J. Fluid Mech.* **629**, 375–385.

Picciotto, M., Marchioli, C. & Soldati, A. 2005 Characterization of near-wall accumulation regions for inertial particles in turbulent boundary layers. *Phys. Fluids* **17**, 098101.

Qureshi, N. M., Bourgoin, M., Aaudet, C., Cartellier, A. & Gagne, Y. 2007 Turbulent transport of material particles: an experimental study of finite size effects. *Phys. Rev. Lett.* **99**, 184502.

Reynolds, A. M. 2003 On the application of nonextensive statistics to Lagrangian turbulence. *Phys. Fluids* **15**, L1–L4.

Reynolds, A. M., Mordant, N., Crawford, A. M. & Bodenschatz, E. 2005 On the distribution of Lagrangian accelerations in turbulent flows. *New J. Phys.* **7**, 58.

Rouson, D. W. I. & Eaton, J. K. 2001 On the preferential concentration of solid particles in turbulent channel flow. *J. Fluid Mech.* **428**, 149–169.

Salazar, J. P. L. C. & Collins, L. R. 2009 Two-particle dispersion in isotropic turbulent flows. *Annu. Rev. Fluid Mech.* **41**, 405–432.

Schiller, L. & Neumann, A. 1933 Uber die grundlegenden berechungen bei der schwer kraftaufbereitung. *Ver. Dtsch. Ing.* **77**, 318.

Soldati, A. & Banerjee, S. 1998 Turbulence modification by large-scale organized electrohydrodynamic flows. *Phys. Fluids* **10**, 1742–1756.

Sundaram, S. & Collins, L. R. 1997 Collision statistics in an isotropic, particle-laden turbulent suspension. Part I. Direct numerical simulations. *J. Fluid Mech.* **335**, 75–109.

Sundaram, S. & Collins, L. R. 1999 A numerical study of the modulation of isotropic turbulence by suspended particles. *J. Fluid Mech.* **379**, 105–143.

Toschi, F. & Bodenschatz, E. 2009 Lagrangian properties of particles in turbulence. *Annu. Rev. Fluid Mech.* **41**, 375–404.

Volk, R., Calzavarini, E., Verhille, G., Lohse, D., Mordant, N., Pinton, J.-F. & Toschi, F. 2008*a* Acceleration of heavy and light particles in turbulence: comparison between experiments and direct numerical simulations. *Physica* D*: Nonlinear Phenom.* **237**, 2084–2089.

Volk, R., Mordant, N., Verhille, G. & Pinton, J.-F. 2008*b* Laser Doppler measurement of inertial particle and bubble accelerations in turbulence. *Eur. Phys. Lett.* **81**, 34002.

Voth, G. A., La Porta, A., Crawford, A. M., Alexander, J. & Bodenschatz, E. 2002 Measurement of particle accelerations in fully developed turbulence. *J. Fluid Mech.* **469**, 121–160.

Voth, G. A., La Porta, A., Crawford, A. M., Bodenschatz, E. & Alexander, J. 2001 A silicon strip detector system for high resolution particle tracking in turbulence. *Rev. Sci. Instrum.* **72**, 4348–4353.

Wang, L. P. & Maxey, M. R. 1993 Settling velocity and concentration distribution of heavy particles in homogeneous isotropic turbulence. *J. Fluid Mech.* **256**, 27–68.

Xu, H., Bourgoin, M., Ouellette, N. T. & Bodenschatz, E. 2006 High order Lagrangian velocity statistics in turbulence. *Phys. Rev. Lett.* **96**, 024503.